

## Article

# Hierarchical Ultrathin Layered GO-ZnO@CeO<sub>2</sub> Nanohybrids for Highly Efficient Methylene Blue Dye Degradation

Marimuthu Karpuraranjith <sup>1,\*</sup>, Yuanfu Chen <sup>1,2,\*</sup>, Ramadoss Manigandan <sup>1</sup>, Katam Srinivas <sup>1</sup> and Sivamoorthy Rajaboopathi <sup>3</sup>

<sup>1</sup> School of Integrated Circuit Science and Engineering, State Key Laboratory of Electronic Thin Films and Integrated Devices, University of Electronic Science and Technology of China, Chengdu 610054, China

<sup>2</sup> School of Science and Institute of Oxygen Supply, Tibet University, Lhasa 850000, China

<sup>3</sup> Department of Chemistry, Government Arts College for Women, Sivagangai 630561, India

\* Correspondence: ranjith3389@gmail.com (M.K.); yfchen@uestc.edu.cn (Y.C.); Tel.: +86-028-83202710 (Y.C.)

**Abstract:** Highly efficient interfacial contact between components in nanohybrids is a key to achieving great photocatalytic activity in photocatalysts and degradation of organic model pollutants under visible light irradiation. Herein, we report the synthesis of nano-assembly of graphene oxide, zinc oxide and cerium oxide (GO-ZnO@CeO<sub>2</sub>) nanohybrids constructed by the hydrothermal method and subsequently annealed at 300 °C for 4 h. The unique graphene oxide sheets, which are anchored with semiconducting materials (ZnO and CeO<sub>2</sub> nanoparticles), act with a significant role in realizing sufficient interfacial contact in the new GO-ZnO@CeO<sub>2</sub> nanohybrids. Consequently, the nano-assembled structure of GO-ZnO@CeO<sub>2</sub> exhibits a greater level (96.66%) of MB dye degradation activity than GO-ZnO nanostructures and CeO<sub>2</sub> nanoparticles on their own. This is due to the thin layers of GO-ZnO@CeO<sub>2</sub> nanohybrids with interfacial contact, suitable band-gap matching and high surface area, preferred for the improvement of photocatalytic performance. Furthermore, this work offers a facile building and cost-effective construction strategy to synthesize the GO-ZnO@CeO<sub>2</sub> nanocatalyst for photocatalytic degradation of organic pollutants with long-term stability and higher efficiency.

**Keywords:** GO-ZnO@CeO<sub>2</sub>; nanostructures; interfacial contact; suitable band-gap matching; photocatalytic degradation



**Citation:** Karpuraranjith, M.; Chen, Y.; Manigandan, R.; Srinivas, K.; Rajaboopathi, S. Hierarchical Ultrathin Layered GO-ZnO@CeO<sub>2</sub> Nanohybrids for Highly Efficient Methylene Blue Dye Degradation. *Molecules* **2022**, *27*, 8788. <https://doi.org/10.3390/molecules27248788>

Academic Editors: Giuseppe Cirillo and Igor Djerdj

Received: 31 October 2022

Accepted: 8 December 2022

Published: 11 December 2022

**Publisher's Note:** MDPI stays neutral with regard to jurisdictional claims in published maps and institutional affiliations.



**Copyright:** © 2022 by the authors. Licensee MDPI, Basel, Switzerland. This article is an open access article distributed under the terms and conditions of the Creative Commons Attribution (CC BY) license (<https://creativecommons.org/licenses/by/4.0/>).

## 1. Introduction

In recent decades, global conservational circumstances have changed with rapid world development, creating new research topics. There has been an increase in the growth of several industries, such as automobile, electronic, furniture and textile dyeing production. Previously, manufacturing companies discharged color and colorless pollutants into wastewater. Water treatment has widespread research opportunities to limit this. Finding a simple, cost-effective and highly efficient route to eliminate industrial contaminants from wastewater is an exciting environmental research topic [1,2].

The chosen semiconducting materials have more significant factors that can influence the photo-catalytic reaction of nanomaterials, such as high electron–hole pair lifetime, being non-toxic, nanostructure, more active surface area, interface contact and suitable band gap. Generally, metal oxide and metal chalcogenide nanomaterials, such as cerium oxide (CeO<sub>2</sub>), iron oxide (Fe<sub>2</sub>O<sub>3</sub>), titanium oxide (TiO<sub>2</sub>), tin oxide (SnO<sub>2</sub>), zinc oxide (ZnO), tin sulfide (SnS) and zinc sulfide (ZnS) are the most widespread semiconducting nanomaterials that have been used in catalytic reactions previously [3–5]. These semiconducting catalysts have some restrictions on the improvement of catalytic activity under visible light irradiation. The ZnO and TiO<sub>2</sub> nanomaterials have a wide-band energy gap in the UV region. It can be assumed that approximately 10% of solar energy will be absorbed with these materials, making them not suitable for practical applications [6].

Nowadays, rare-earth metal oxides have been established. Cerium (Ce) typically has two different forms of oxide: cerium sesquioxide ( $\text{Ce}_2\text{O}_3$ ) and cerium dioxide ( $\text{CeO}_2$ ), respectively. Moreover,  $\text{CeO}_2$  has fluorite structure (FCC) and higher stability than  $\text{Ce}_2\text{O}_3$ . Cerium belongs to a rare-earth family and is more abundant than tin and copper [7,8]. High abundance makes this material scientifically significant, with an extensive range in several applications such as biotechnology, oxygen permeation membrane systems, environmental chemistry, fuel cells, glass-polishing materials, low-temperature water–gas shift reaction, auto-exhaust catalysts, oxygen sensors and electrochromic thin-film applications, as well as photocatalysts and medicine [9,10].

Typically, the photocatalytic activity of rare-earth family materials is enhanced by doping constituents for modification of the energy band gap. Nevertheless, such doping constituents characteristically produce the subordinate pollutants [11,12]. Hence, they are frequently attached to another semiconducting material that can increase the electron–hole pair lifetime. Recently, several studies have examined the effectiveness of combining carbon with metal oxides, for example, carbon nanotubes (CNTs), graphene oxide (GO) and reduced graphene oxide (rGO), as an effective way to decrease the electron–hole pair recombination rate and avoid the accumulation of metal oxide particles [13–15].

Therefore, various combined metal oxides, such as  $\text{TiO}_2@\text{GO}$ ,  $\text{TiO}_2@\text{CNT}$ ,  $\text{ZnO}@\text{RuO}_2$ ,  $\text{ZnO}@\text{rGO}$  and  $\text{ZnO}@\text{CNT}$ , offer great photocatalytic performance while reducing the recombination rate and spreading the energy range in which photoexcitation occurs. However, the mechanism and catalytic effectiveness underlying graphene oxide–ZnO nanosheet activity are not well understood [16–19]. We think that it is reasonable for the photocatalytic activity of  $\text{CeO}_2$  nanoparticles to be improved by nano-assembly on graphene oxide–ZnO nanosheets. Recently, with this in mind, our associates have conducted a great deal of correlated research; for example, highly efficient photo-degradation was reported by R. Jeyagopal et al. [20] for the  $\text{CoSnS}@\text{CNT}$  hybrid catalyst using the hydrothermal method. Likewise, M. Karpuraranjith et al. used the hydrothermal method for enhancement of photocatalytic degradation with hexagonal SnSe nanoplate @  $\text{SnO}_2$ -CNTs [21] and better photocatalytic activity using the hydrothermal method was reported by B. Wang et al. [22] with an rGO wrapped trimetallic sulfide nanowire hybrid catalyst.

To focus on such problems, we used a cost-effective and facile hydrothermal strategy to synthesize GO–ZnO@ $\text{CeO}_2$  nanohybrids, and then investigated using several instrumental techniques such as HR-TEM, FT-IR, XRD, UV–visible DRS with band gap,  $\text{N}_2$ -adsorption–desorption isotherm and mass spectroscopy. Furthermore, we conducted a systematic study of the degradation of methylene blue pollutant, which is effectively attributed to the typical nanosheets, interfacial contact, high surface area and band-gap matching.

## 2. Results and Discussion

### 2.1. Morphological Characterization

The surface morphological features that have been studied by HR-TEM performance are presented in Figure 1a–c. Fortunately, the recombination of semiconducting metal oxides (ZnO and  $\text{CeO}_2$ ) and graphene oxide by annealed and hydrothermal methods resulted in a unique well-defined ultrathin 2D nanohybrid layered structure with ZnO and  $\text{CeO}_2$  nanoparticles well dispersed on restacked structures of GO nanosheets. In addition, Figure 1d shows high-resolution TEM images of GO–ZnO@ $\text{CeO}_2$  nanostructures being established by selected area electron diffraction (SAED) patterns; the different crystallographic locations were seen in ZnO nanoparticles for (100), (002), (110) and (103), and  $\text{CeO}_2$  nanoparticles for (200) and (111), respectively [23]. Moreover, the ZnO nanoparticles develop an interlayer spacing of  $\sim 0.25$  nm and the theoretical d-spacing indicates that the hexagonal crystal plane (002) and  $\text{CeO}_2$  make an efficiently porous layered assembly which has an interlayer distance  $\sim 0.31$  nm and cubic crystal plane (111) [24]. The ultrathin layered structure of GO–ZnO@ $\text{CeO}_2$  may be favorable for the lower band gap and good surface activity concluded the photocatalytic reaction, further supported by the XRD results. In

addition, the interfacial coupling between the ZnO@CeO<sub>2</sub> nanostructure and graphene oxide sheet materials obviously plays a significant role in the photocatalytic efficiency.

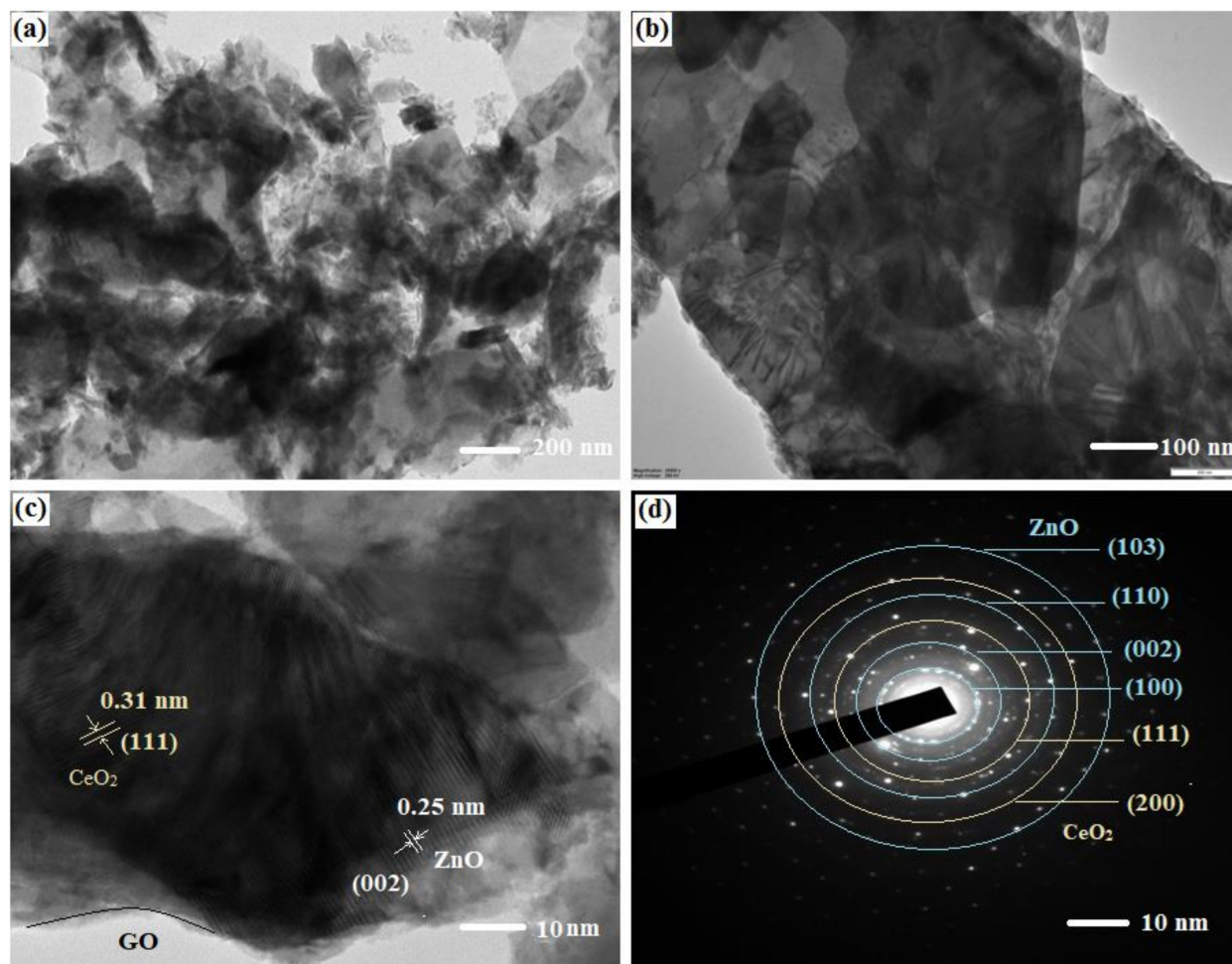


**Figure 1.** HR-TEM images of (a–c) GO-ZnO@CeO<sub>2</sub> nanohybrids and (d) SAED pattern.

## 2.2. Structural Characterizations

The functional group information of the CeO<sub>2</sub>, GO-ZnO, ZnO@CeO<sub>2</sub> and GO-ZnO@CeO<sub>2</sub> samples are shown in Figure 2. The FTIR spectrum of CeO<sub>2</sub> displays several peaks at 3410, 2924, 2856, 1742, 1625, 1537, 1344, 1049, 958, 875 and 537 cm<sup>-1</sup>, which agrees with the characteristic chemical components in the stretching vibrations of O-H bonds and metal–oxygen bonds [25].

GO-ZnO nanoparticles exhibit various peaks that expose the existence of oxygen in the samples and additionally display several peaks at 1797, 1443 and 1048 cm<sup>-1</sup> which correspond to the functional groups of carbonyls (C=O), tertiary (C-OH) and alkoxy (or) epoxy (C-O), respectively. The main characteristic peaks at 3431 cm<sup>-1</sup> may be accredited to the stretching vibration of (O-H) hydroxyl groups. Furthermore, the obtained peak at 1630 cm<sup>-1</sup> may denote the remaining sp<sup>2</sup> bonds of graphene oxide [26]. The FT-IR spectrum of ZnO nanoparticles has a peak at 428 cm<sup>-1</sup> that signifies the stretching vibration of metal–oxygen bonds.

The characteristic peaks of ZnO@CeO<sub>2</sub> nanoparticles, compared to CeO<sub>2</sub>, show few new peaks attributed to the assembly of both (ZnO and CeO<sub>2</sub> peaks), shifted to 22 cm<sup>-1</sup>. It is interesting to note that GO-ZnO@CeO<sub>2</sub> nanohybrids, compared to GO-ZnO, display some new peaks attributed to the mixture of CeO<sub>2</sub> and the metal oxide; the peak seems to have shifted to ~47 cm<sup>-1</sup>. A strong peak at 422 cm<sup>-1</sup> is attributed to the vibration of the Zn–O bond in ZnO and the peak at 475 cm<sup>-1</sup> is attributed to the vibration of the Ce–O

bond in  $\text{CeO}_2$ , due to the interaction of  $\text{Zn}^{2+}$  and  $\text{Ce}^{4+}$  ions with graphene oxide. Therefore, the results obviously show that the co-existence of GO, an inorganic counterpart of metal oxides, can be an effective cover on a nanohybrid structured graphene oxide surface.

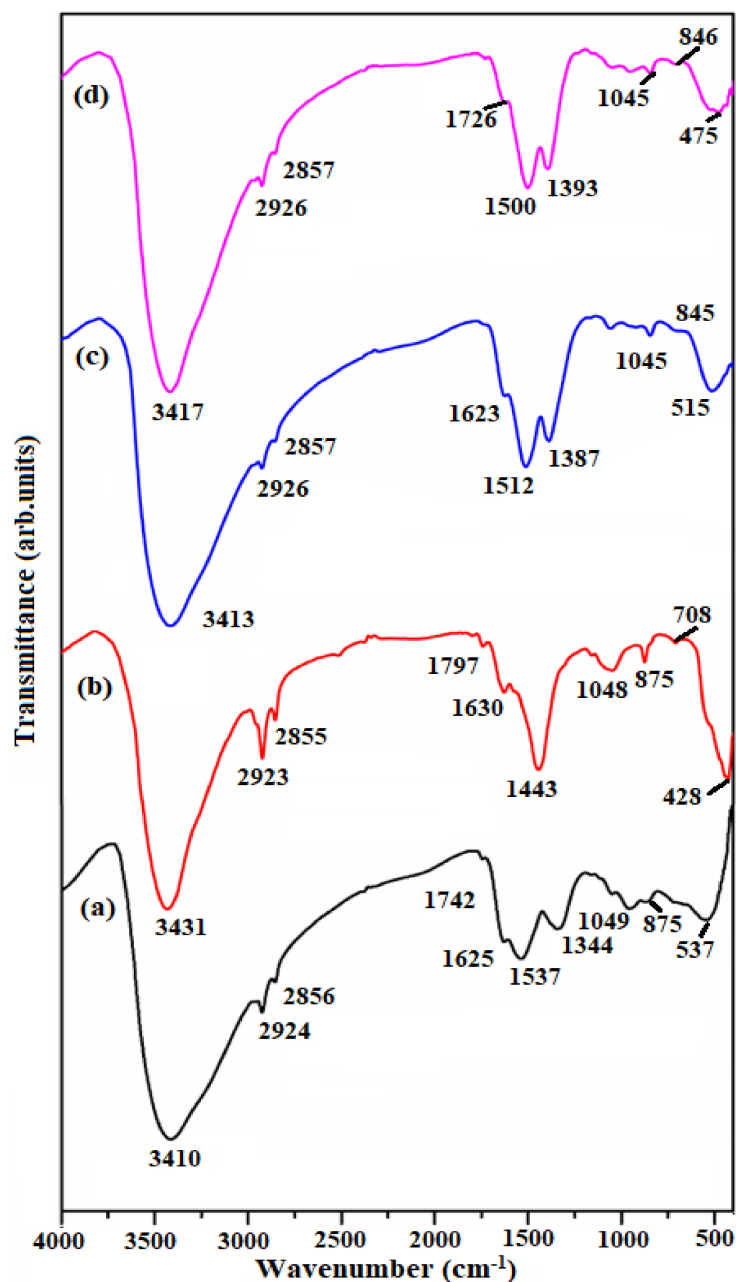
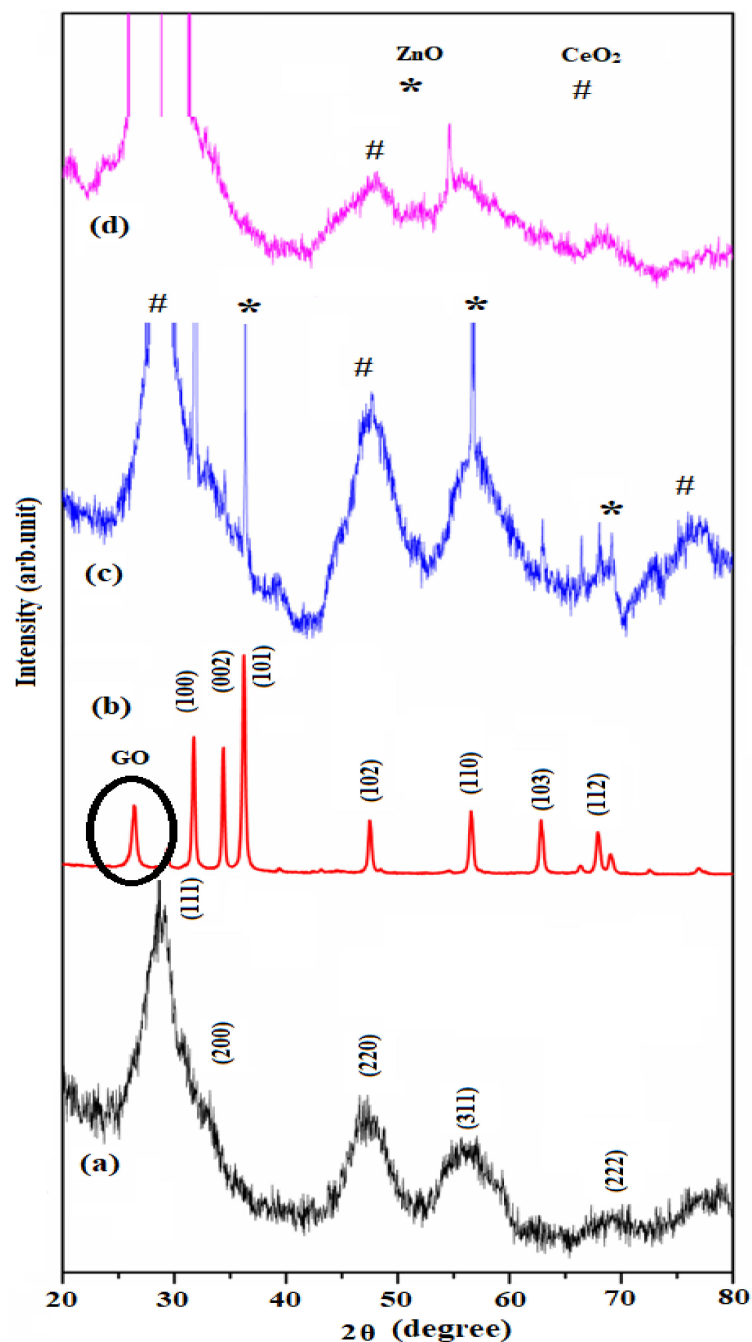


Figure 2. FT-IR analysis of (a)  $\text{CeO}_2$ , (b) GO-ZnO, (c)  $\text{ZnO@CeO}_2$  and (d) GO-ZnO@ $\text{CeO}_2$ .

The structural information of  $\text{CeO}_2$ , GO-ZnO,  $\text{ZnO@CeO}_2$  and GO-ZnO@ $\text{CeO}_2$  nanohybrids were investigated by X-ray diffraction analysis and their results are revealed in Figure 3. X-ray diffraction patterns of cubic structure  $\text{CeO}_2$  (JCPDS cars no. 34-0394) exhibit diffraction peak  $2\theta$  values at  $28.6^\circ$ ,  $33.5^\circ$ ,  $46.7^\circ$ ,  $56.8^\circ$  and  $68.7^\circ$ , which is well indexed to the lattice planes corresponding to (111), (200), (220), (311) and (222), respectively [27]. The powder XRD pattern of GO-ZnO nanohybrids was obtained in the diffraction peaks at  $2\theta = 31.3^\circ$ ,  $34.1^\circ$ ,  $36.3^\circ$ ,  $47.8^\circ$ ,  $56.7^\circ$ ,  $62.8^\circ$  and  $69.4^\circ$  corresponding to the (100), (002), (101), (102), (110), (103) and (112) characteristic crystal diffraction planes of ZnO (hexagonal structure) as (JCPDS-36-1451) confirmed [28,29]. In addition, a low intensity diffraction

peak was observed, the  $2\theta$  value at  $26.4^\circ$  well matching the lattice plane (002) of graphene oxide [30], confirming the existence of GO-ZnO nanostructures.



**Figure 3.** X-ray diffraction analysis of (a)  $\text{CeO}_2$ , (b) GO-ZnO, (c)  $\text{ZnO@CeO}_2$  and (d) GO-ZnO@ $\text{CeO}_2$ .

It is interesting to note that the X-ray diffraction patterns of  $\text{ZnO@CeO}_2$  and GO-ZnO@ $\text{CeO}_2$  nanohybrids, revealed in several diffraction planes of the cubic structure of  $\text{CeO}_2$  and hexagonal wurtzite structure of ZnO nanoparticles, were confirmed and no characteristic peaks of graphene oxide were detected, indicating the influence of metal oxide nanoparticles. Moreover, XRD analysis reveals a good crystalline phase for ZnO and  $\text{CeO}_2$  nanomaterials using the hydrothermal method, which is reliable through TEM analysis results.

### 2.3. Optical and Surface Area Characterization

UV–visible absorbance spectra and suitable band-gap matching studies were investigated for insight into the photocatalytic reaction. The absorbance spectrum of CeO<sub>2</sub>, GO-ZnO, ZnO@CeO<sub>2</sub> and GO-ZnO@CeO<sub>2</sub> nanohybrids are shown in Figure 4A. A broad absorption peak is noticed at 350 nm in the absorption spectra of CeO<sub>2</sub>. The absorption edges of GO-ZnO at 360 nm and GO-ZnO@CeO<sub>2</sub> appearing at 356 nm were blue shifted towards a lower wavelength, which suggests a reduction in the band gap from the introduction of GO [31–33]. Furthermore, a characteristic absorption through a powerful transition in the UV region was detected in the above samples, exchangeable with the intrinsic band absorption of ZnO@CeO<sub>2</sub> for electron shift from the valence band into the conduction band [34].

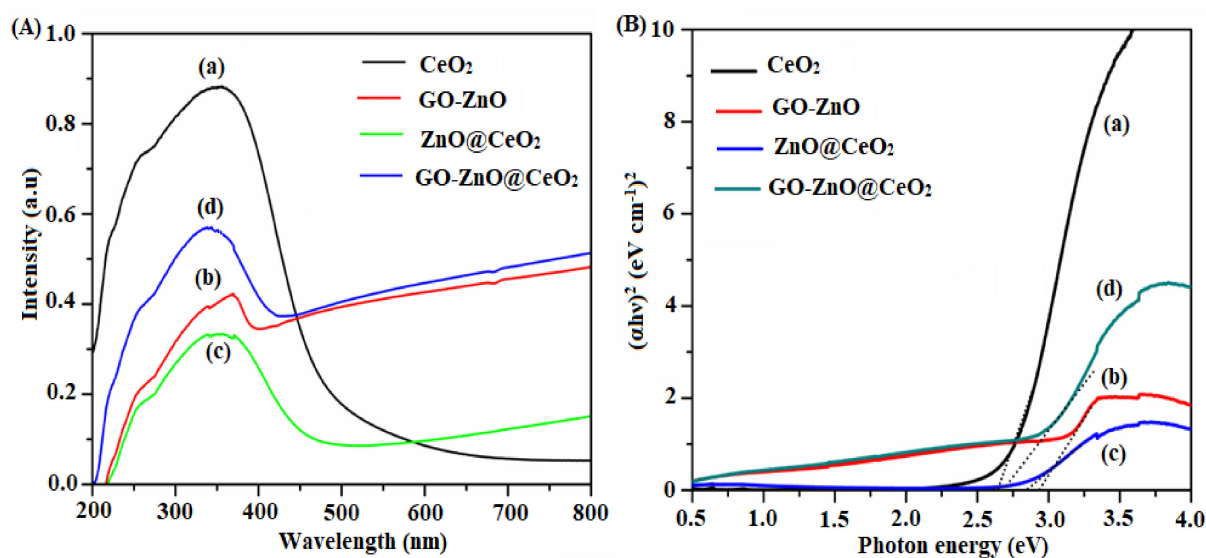


**Figure 4.** (A) UV–visible absorbance spectra and (B) energy band gap of (a) CeO<sub>2</sub>, (b) GO-ZnO, (c) ZnO@CeO<sub>2</sub> and (d) GO-ZnO@CeO<sub>2</sub>.

In Figure 4B, the optical energy gap ( $E_g$ ) of the nanohybrids was determined via Tauc's plots,  $\alpha(h\nu) = A(h\nu - E_g)^{n/2}$ . The estimated energy gaps of CeO<sub>2</sub>, GO-ZnO, ZnO@CeO<sub>2</sub> and GO-ZnO@CeO<sub>2</sub> nanohybrids were calculated to be 2.63, 2.92, 2.84 and 2.70 eV, respectively. Furthermore, lowering the band-gap energy of GO-ZnO@CeO<sub>2</sub> is reliable through the larger level reactive in the photocatalytic reaction, and it might remain attributed to the building of interfacial contact between ZnO@CeO<sub>2</sub> nanostructures and GO nanosheets.

The N<sub>2</sub> adsorption/desorption isotherms for the GO-ZnO and GO-ZnO@CeO<sub>2</sub> nanohybrids exhibit typical IV isotherm (at high  $P/P_0$ ) according to the IUPAC organization. As shown in Figure 5a,b, the BET surface area and pore volume for the GO-ZnO and GO-ZnO@CeO<sub>2</sub> nanohybrids were calculated to be (23.8 m<sup>2</sup>/g and 0.166 cc/g) and (47.4 m<sup>2</sup>/g and 0.237 cc/g), respectively. These results are more helpful for enhancement of the photocatalytic activity.

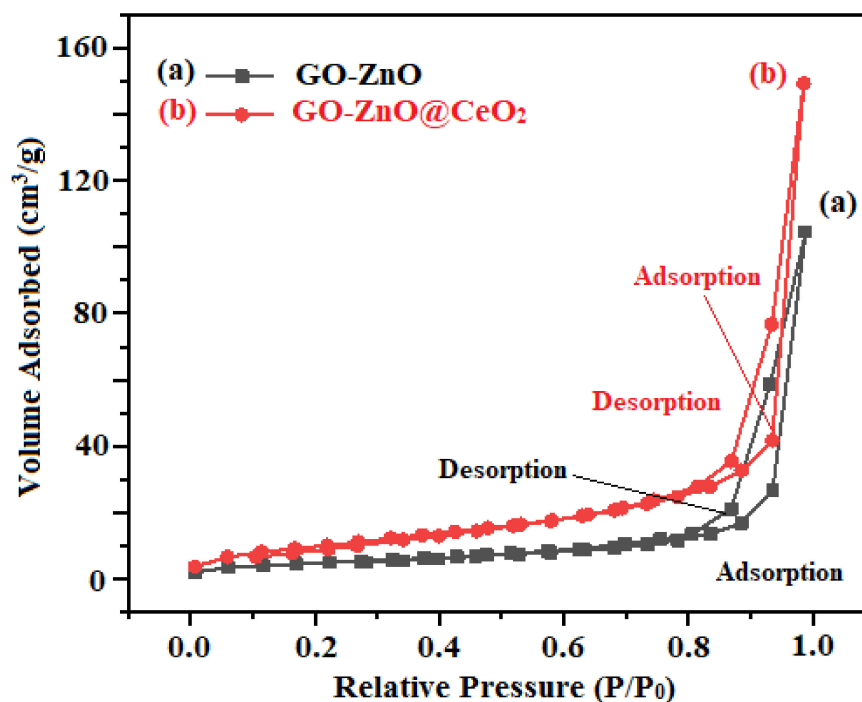
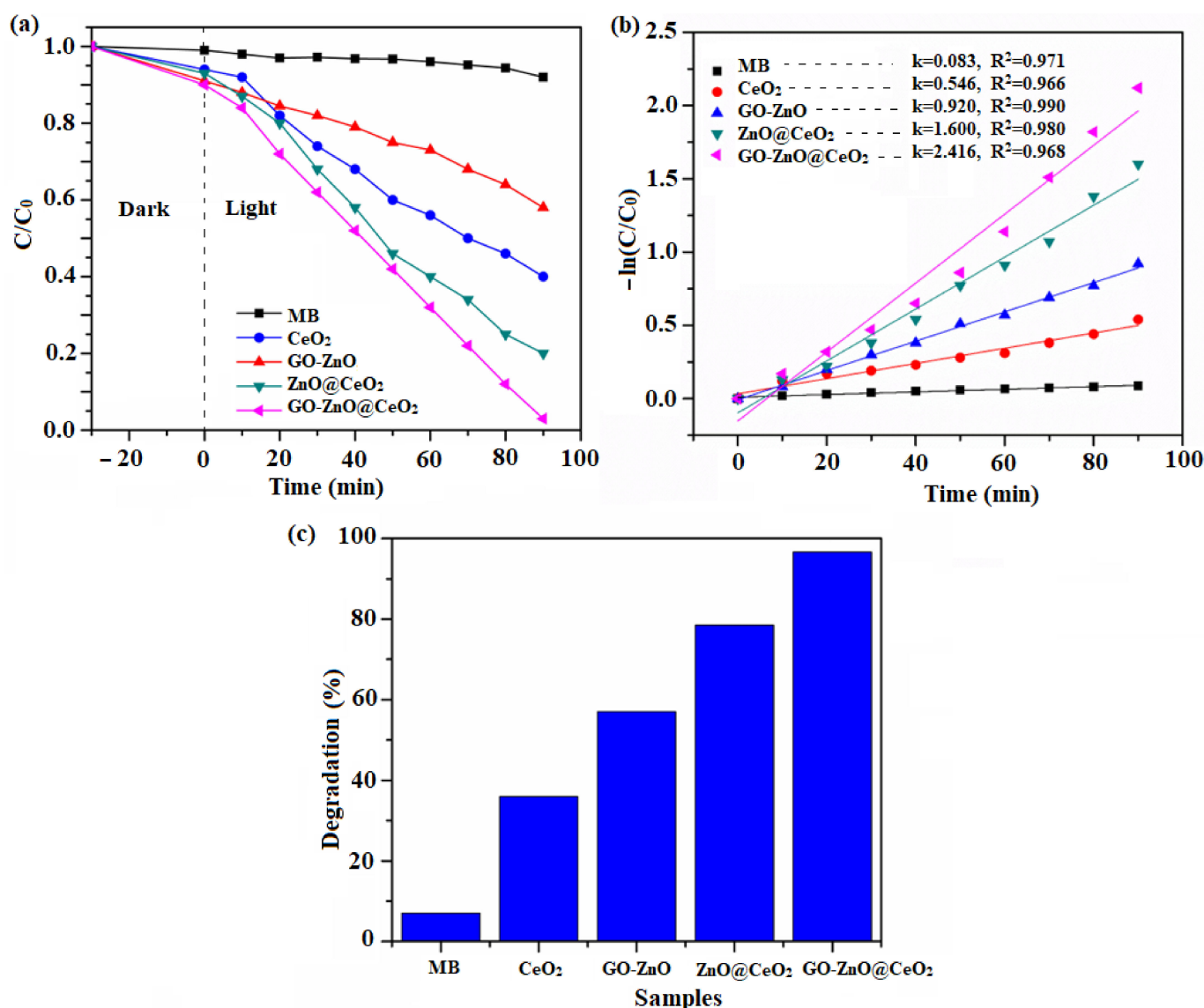


Figure 5.  $N_2$  adsorption/desorption isotherms of (a) GO-ZnO and (b) GO-ZnO@CeO<sub>2</sub>.

#### 2.4. Photocatalytic Dye Degradation

The photocatalytic performance of as-prepared CeO<sub>2</sub>, GO-ZnO, ZnO@CeO<sub>2</sub> and GO-ZnO@CeO<sub>2</sub> nanohybrid photocatalysts were examined using methylene blue dye by UV–visible spectroscopy. Investigating the presence of the photocatalyst, it can be seen that the dye absorption curve against time decreases in peak intensity under visible light conditions. Figure 6a, without photocatalyst, exhibits the MB dye absorption peak at 664 nm and no significant change is seen up to the 90 min interval. Correspondingly, introducing the nanocatalyst shows a large level decrease in the peak intensity. Photocatalytic performance was demonstrated by the self-degradation achieved (7.8%) by the MB dye. The photodegradation of the MB dye in the presence of a photocatalyst, for instance CeO<sub>2</sub> (36.82%), GO-ZnO (57.43%) and ZnO@CeO<sub>2</sub> (78.52%), might be degraded for 90 min. The obvious photodegradation effectiveness of GO-ZnO nanostructures was enhanced; the degradation efficiency achieved (96.66%) by the doping of CeO<sub>2</sub> nanoparticles was larger than for the GO-ZnO and ZnO@CeO<sub>2</sub> nanostructures. The photocatalytic activities of nanohybrids, after 90 min duration, were obtained in the order of GO-ZnO@CeO<sub>2</sub> > ZnO@CeO<sub>2</sub> > GO-ZnO > CeO<sub>2</sub>; there may be a combined effect caused by the graphene oxide making nano-structures on ZnO@CeO<sub>2</sub> and possibly reducing the electron–hole recombination, enhancing the degradation efficiency.



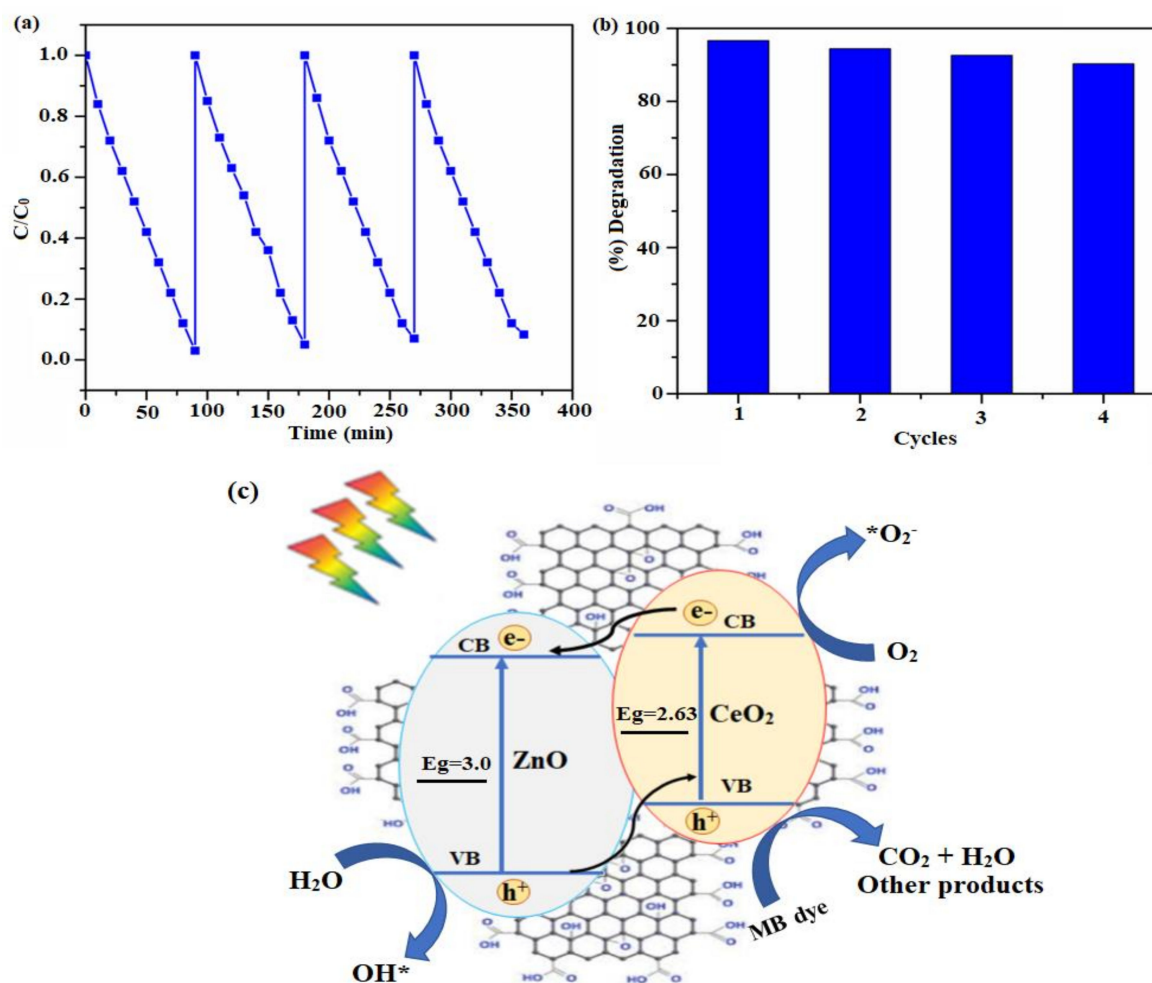
**Figure 6.** MB dye degradation. (a) Plots of irradiation time vs. efficiency, (b) pseudo-first-order kinetics and (c) degradation (%).

Figure 6b, the photodegradation reactions of methylene blue, can be evaluated by using Langmuir Hinshelwood pseudo-first-order kinetics. Interestingly, the rate constant (k) for GO-ZnO@ $CeO_2$  is the fastest kinetics value at  $2.416 \text{ min}^{-1}$  and is 1.5 times higher than those of  $ZnO@CeO_2$  ( $1.603 \text{ min}^{-1}$ ), GO-ZnO ( $0.924 \text{ min}^{-1}$ ) and  $CeO_2$  ( $0.546 \text{ min}^{-1}$ ), respectively.

Figure 6c exhibits the total percentage of photodegradation efficiency, completing the response on the 90 min interval, for the photocatalytic performance of MB dye (36.82, 57.43, 78.52 and 96.66%) obtained with the corresponding nanohybrid photocatalyst of  $CeO_2$ , GO-ZnO,  $ZnO@CeO_2$  and GO-ZnO@ $CeO_2$ , respectively. Thus, the consequences suggest that the combination effect of GO-ZnO@ $CeO_2$  can effectively induce the photocatalytic activity of GO and  $ZnO@CeO_2$  through suitable band-gap matching and interfacial contact on the nanosheets. The achieved degradation efficiency outcomes were compared to other hybrid catalysts and shown in (Table 1) [35–38]; the GO-ZnO@ $CeO_2$  nanohybrid catalyst displayed highly effective photocatalytic results. Furthermore, the photocatalytic recyclability of the GO-ZnO@ $CeO_2$  nanohybrid catalyst was also examined and the results revealed in Figure 7a,b. The degradation activity of MB dye molecules demonstrates the four repeated cycles achieving about ~96.66 to 90.62% within 90 min, which suggests that GO-ZnO@ $CeO_2$  is confirmed to have good stability as well as recyclability for the degraded MB dye.

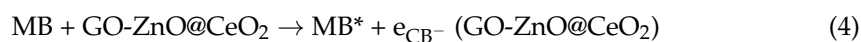
**Table 1.** Comparison of previously reported catalysts with our nano hybrid catalyst.

Photocatalyst	Method	Degradation (%)	Degradation Target	Times (min)	Ref.
TiO <sub>2</sub> /MoS <sub>2</sub> /RGO	Hydrothermal	92.4	MB	100	[35]
CeO <sub>2</sub> /SnO <sub>2</sub> /RGO	Hydrothermal	95.0	MB	90	[36]
gCN@TiO <sub>2</sub> /MoS <sub>2</sub>	Hydrothermal	94.0	MB	60	[37]
SnO <sub>2</sub> /MoS <sub>2</sub> /RGO	Hydrothermal	90.0	MB	75	[38]
GO/ZnO@CeO <sub>2</sub>	Hydrothermal	96.6	MB	90	This work

**Figure 7.** (a) Stability, (b) recyclability and (c) photocatalytic mechanism using GO-ZnO@CeO<sub>2</sub>.

Pleasingly, the photodegradation mechanism is demonstrated in Figure 7c. An MB pollutant molecule in the aqueous solution and the GO-ZnO@CeO<sub>2</sub> nano hybrid photocatalyst were treated using UV or visible light, and produced the electron-hole pairs. The produced holes and electrons are strong oxidizing and reducing agents, respectively. The produced electrons in the conduction band respond with O<sub>2</sub> molecules to form a superoxide radical ion (\*O<sub>2</sub><sup>-</sup>). The produced holes in the valence band respond with H<sub>2</sub>O molecules, resulting in the creation of (\*OH) hydroxyl radical. The graphene oxide acts as an electron-hole pair separation, to avoid their recombination, and a good electron acceptor. Lastly, the \*OH radicals, which can mineralize the organic molecules and oxidize, respond with MB molecules, which results in the making of various species, such as CO<sub>2</sub>, water and other intermediate products [39–42], as in the following equations:





To understand the intermediate product degradation of MB dye, different stages were further validated by mass spectroscopy. The test was controlled by using ESI-MS in the (+ve) ion scanning mode to detect the ( $m/z$ ) mass-to-charge ratio of the samples. The mechanistic pathway of the photodegradation of MB dye to form intermediates using the GO-ZnO@CeO<sub>2</sub> nanohybrid photocatalyst is shown in Figure 8a,b. The molecular weight of methylene blue (319.85) was detected, but the representative high-intensity peak was observed at 284 ( $m/z$ ), due to the removal of (Cl<sup>-</sup>) ions [43,44]. In consequence of the degradation of MB dye, the photogenerated active species such as <sup>\*</sup>OH could attack the essential carbon atom of MB to adeptly decolorize the dye molecule.

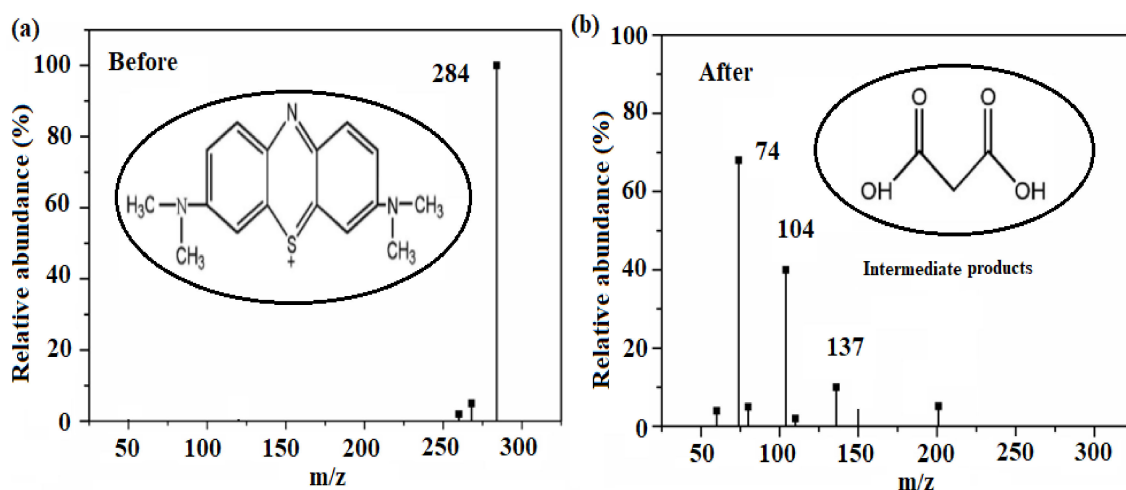
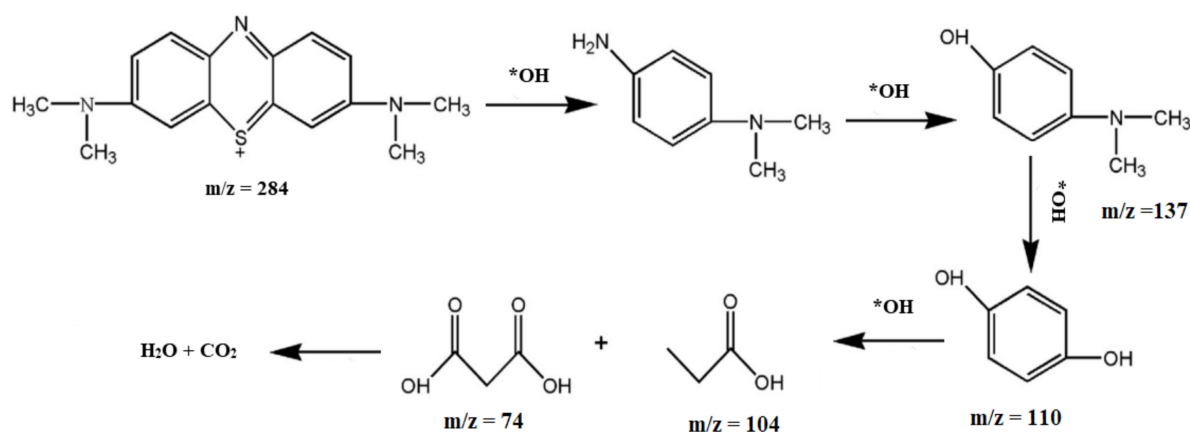


**Figure 8.** ESI-MS analysis of MB dye degradation (a) before and (b) after intermediate products.

Noticeably, after 90 min of photodegradation, the constituents have gone; the preliminary step of the MB degradation would attack the <sup>\*</sup>OH radicals that adapt the C-S<sup>+</sup>=C and C=N-C bonds to the C-SH (=O)<sub>2</sub>-C and C-NH-C. The dye degradation intermediate products obtained at ( $m/z$ ) 202, 137, 110, 104 and 74 were detected. Since the visual detection and investigative information, it is obvious that the MB dye has been completely degraded into different compounds via the cleavage of the (C-N) azo group bond. Hereafter, in the experimental procedure, the MB dye was oxidized and mineralized into small molecules, such as CO<sub>2</sub>, H<sub>2</sub>O and other intermediate constituents (Scheme 1). The methylene blue degradation intermediate product confirmed the results and agreed with the previously described literature on dye degradation performance [45,46].



**Scheme 1.** Possible organic intermediates of the methylene blue dye degradation.

### 3. Experimental Details

#### 3.1. Materials

Cerium nitrate ( $\text{Ce}(\text{NO}_3)_3 \cdot 6\text{H}_2\text{O}$ ), zinc nitrate ( $\text{Zn}(\text{NO}_3)_2 \cdot 6\text{H}_2\text{O}$ ), graphite powder, hydrochloric acid (HCl), hydrogen peroxide ( $\text{H}_2\text{O}_2$ ), nitric acid ( $\text{HNO}_3$ ), sulfuric acid ( $\text{H}_2\text{SO}_4$ ), sodium thiosulfate ( $\text{Na}_2\text{S}_2\text{O}_3 \cdot 5\text{H}_2\text{O}$ ), sodium nitrate ( $\text{NaNO}_3$ ) and potassium permanganate ( $\text{KMnO}_4$ ) were purchased from a Nice chemical factory, Mumbai, India. Methylene blue ( $\text{C}_{16}\text{H}_{18}\text{ClN}_3\text{S}_2\text{O}_2$ ; MW 319.85) was obtained from the Merck chemical industry, Mumbai, India. All the chemicals and reagents have an AR grade and are used without any further process. All the experimental work also used Millipore water.

#### 3.2. Preparation of Graphene Oxide (GO) Nanosheets

The graphene oxide nanosheet (GO) was synthesized from graphite powder by adapted Hummer's technique; details were discussed in a previous report [26].

#### 3.3. Synthesis of Ultrathin Layered GO-ZnO@CeO<sub>2</sub> Nanohybrids

In a typical experiment, 250 mg of graphene oxide powder was homogeneously dispersed in a 25 mL ethanol and water mixture. In addition, the solution was kept under ultrasonic for 60 min to get a consistent solution at room temperature (A). Meanwhile, equal volumes of 0.5 M zinc nitrate and 0.5 M cerium nitrate solution were continuously stirred for 30 min to obtain a homogenous solution (B). Subsequently, A and B solutions were mixed in a single bath and stirred for 10 min to achieve a dispersal mixture, and newly arranged 25 mL of 1 M sodium hydroxide solution was added drop by drop into the dispersion mixture. After that, the reaction bath product was transferred to a 100 mL Teflon-lined stainless-steel autoclave and put into a hot air oven kept at 180 °C for 1 day. The resultant product was cooled down at room temperature and then washed through a water/ethanolic mixture several times. It was filtered in a suction pump and dried at 80 °C for 12 h. Finally, the obtained powder was annealed using a muffle furnace at 300 °C heating for 4 h and designated as GO-ZnO@CeO<sub>2</sub> nanohybrids. In a similar way to prepared GO-ZnO without CeO<sub>2</sub>, ZnO@CeO<sub>2</sub> was prepared without graphene oxide.

#### 3.4. Characterizations

The functional groups of graphene oxide, zinc oxide and cerium oxide were characterized and identified by FT-IR spectroscopic analysis using Detector-TGS with KBr pellets (FT/IR-4600 type). Powder-XRD of the GO-ZnO@CeO<sub>2</sub> nanostructures was approved with X-ray diffractometer (model XPERT-PRO). Morphological construction and shape distribution of the GO-ZnO@CeO<sub>2</sub> nanohybrids were examined by JEOL-2100+ High Resolution Transmission Electron Microscopy (Accelerating Voltage: 200 kV). Optical behavior and suitable band-gap energy of GO-ZnO@CeO<sub>2</sub> were measured by JASCO UV-visible NIR (V-670). The intermediate constituents of the degraded dye molecules were examined

using JEOL GC MATE-II mass spectrometer. Specific surface area and pore volume of the nanohybrids were examined by  $N_2$ -adsorption–desorption isotherm using (Quantachrome Instrument v11.05), Quantachrome Novawin, Boynton Beach, FL, USA.

### 3.5. Photo-Catalytic Experiments

In a distinctive test, the photocatalytic efficiency of synthesized nanohybrid catalyst was examined by methylene blue dye as a model contaminant. About 50 mg nanohybrid catalyst was well spread in 100 mL of MB dye (10 ppm) aqueous solution [21]. Before irradiation, the suspension mixture was magnetically stirred for 30 min to make the adsorption–desorption isotherm equilibrium. Subsequently, the reaction product was subjected to visible light irradiation (UV filter cut off at 400 nm with 350 W Xenon lamp from Juyanguangdian Technology Co., Ltd., Chengdu, China). An amount of 3 mL of the treated solution was taken at different time intervals to analyze the concentration difference of organic dye molecules by UV–visible spectrophotometer in the range from 400 to 800 nm (maximum absorption peak at 664 nm using (INESA L5) from Zhejiang Scientific Instruments Co., Ltd., Zhejiang, China).

## 4. Conclusions

In summary, for the first time, a new GO-ZnO@CeO<sub>2</sub> nanohybrid was synthesized using a hydrothermal method. A variety of techniques were used (FT-IR, XRD, HR-TEM, UV–visible DRS with band gap and BET analysis) to characterize the obtained materials. The GO-ZnO@CeO<sub>2</sub> nanohybrids exhibit excellent photocatalytic performance for the degradation of organic pollutants (96.66%), under visible-light irradiated with favorable cycling stability. Furthermore, it is expected that the present work will offer new prospects for the design of low-cost nanohybrids with efficient photocatalytic activity and upcoming applications in environmental organization.

**Author Contributions:** Conceptualization, Y.C.; Methodology, M.K. and Y.C.; Formal analysis, M.K., R.M., K.S. and S.R.; Investigation, M.K.; Data curation, R.M.; Writing—original draft, M.K.; Supervision, Y.C. All authors have read and agreed to the published version of the manuscript.

**Funding:** The research was supported by the National Natural Science Foundation of China (Grant Nos. 21773024) and China Postdoctoral Science Foundation (Grant No. 2019M653376).

**Institutional Review Board Statement:** Not applicable.

**Informed Consent Statement:** Not applicable.

**Data Availability Statement:** Not applicable.

**Acknowledgments:** The support by Alagappa University for High Resolution Transmission Electron Microscopy is gratefully acknowledged.

**Conflicts of Interest:** The authors declare no conflict of interest.

**Sample Availability:** Samples of the compounds are not available from the authors.

## References

1. An, X.; Shang, Z.; Bai, Y.; Liu, H.; Qu, J. Synergetic Photocatalytic Pure Water Splitting and Self-Supplied Oxygen Activation by 2D WO<sub>3</sub>/TiO<sub>2</sub> Heterostructures. *ACS Sustain. Chem. Eng.* **2019**, *7*, 19902–19909. [[CrossRef](#)]
2. Shao, Y.; Du, J.; Li, H.; Zhao, Y.; Xu, C. Ni<sub>0.37</sub>Co<sub>0.63</sub>S<sub>2</sub>-reduced graphene oxide nanocomposites for highly efficient electrocatalytic oxygen evolution and photocatalytic pollutant degradation. *J. Solid State Electrochem.* **2017**, *21*, 183–192. [[CrossRef](#)]
3. Fernandes, A.; Gagol, M.; Makoś, P.; Khan, J.A.; Boczkaj, G. Integrated photocatalytic advanced oxidation system (TiO<sub>2</sub>/UV/O<sub>3</sub>/H<sub>2</sub>O<sub>2</sub>) for degradation of volatile organic compounds. *Sep. Purif. Technol.* **2019**, *224*, 1–14. [[CrossRef](#)]
4. Ahmed, L.M.; Saaed, S.I.; Marhoon, A.A. Effect of Oxidation Agents on Photo-Decolorization of Vitamin B12 in the Presence of ZnO/UV-A System. *Indones. J. Chem.* **2018**, *18*, 272–278. [[CrossRef](#)]
5. Srinivas, K.; Chen, Y.; Wang, B.; Yu, B.; Wang, X.; Hu, Y.; Lu, Y.; Li, W.; Zhang, W.; Yang, D. Metal–Organic Framework-Derived NiS/Fe<sub>3</sub>O<sub>4</sub> Heterostructure-Decorated Carbon Nanotubes as Highly Efficient and Durable Electrocatalysts for Oxygen Evolution Reaction. *ACS Appl. Mater. Interfaces* **2020**, *12*, 31552–31563. [[CrossRef](#)]

6. Cai, Y.Z.; Cao, W.Q.; Zhang, Y.L.; He, P.; Shu, J.C.; Cao, M.S. Tailoring rGO-NiFe<sub>2</sub>O<sub>4</sub> hybrids to tune transport of electrons and ions for supercapacitor electrodes. *J. Alloys Compd.* **2019**, *811*, 152011. [[CrossRef](#)]
7. Karpuraranjith, M.; Chen, Y.; Ramadoss, M.; Wang, B.; Yang, H.; Rajaboopathi, S.; Yang, D. Magnetically recyclable magnetic biochar graphitic carbon nitride nanoarchitectures for highly efficient charge separation and stable photocatalytic activity under visible-light irradiation. *J. Mol. Liq.* **2021**, *326*, 115315. [[CrossRef](#)]
8. Xu, Y.; Huang, S.; Xie, M.; Li, Y.; Xu, H.; Huang, L.; Zhang, Q.; Li, H. Magnetically separable Fe<sub>2</sub>O<sub>3</sub>/g-C<sub>3</sub>N<sub>4</sub> catalyst with enhanced photocatalytic activity. *RSC Adv.* **2015**, *5*, 95727–95735. [[CrossRef](#)]
9. Ni, X.; Chen, C.; Wang, Q.; Li, Z. One-step hydrothermal synthesis of SnO<sub>2</sub>-MoS<sub>2</sub> composite heterostructure for improved visible light photocatalytic performance. *Chem. Phys.* **2019**, *525*, 110398. [[CrossRef](#)]
10. Wang, G.; Wang, L. Hydrothermal synthesis of hierarchical flower-like  $\alpha$ -CNTs/SnO<sub>2</sub> architectures with enhanced photocatalytic activity. *Fuller. Nanotub. Carbon Nanostruct.* **2019**, *27*, 10–13. [[CrossRef](#)]
11. Liu, F.; Dong, S.; Zhang, Z.; Li, X.; Dai, X.; Xin, Y.; Wang, X.; Liu, K.; Yuan, Z.; Zheng, Z. Synthesis of a well-dispersed CaFe<sub>2</sub>O<sub>4</sub>/g-C<sub>3</sub>N<sub>4</sub>/CNT composite towards the degradation of toxic water pollutants under visible light. *RSC Adv.* **2019**, *9*, 25750–25761. [[CrossRef](#)]
12. Lin, J.; Luo, Z.; Liu, J.; Li, P. Photocatalytic degradation of methylene blue in aqueous solution by using ZnO-SnO<sub>2</sub> nanocomposites. *Mater. Sci. Semicond. Process.* **2018**, *87*, 24–31. [[CrossRef](#)]
13. Khurshid, F.M.; Jeyavelan, M.; Nagarajan, S. Photocatalytic dye degradation by graphene oxide doped transition metal catalysts. *Syn. Met.* **2021**, *278*, 11683. [[CrossRef](#)]
14. Naciri, Y.; Chennah, A.; Jaramillo-Páez, C.; Navío, J.A.; Bakiz, B.; Taoufiq, A.; Ezahri, M.; Villain, S.; Guinneton, F.; Benlhachemi, A. Preparation, characterization and photocatalytic degradation of Rhodamine B dye over a novel Zn<sub>3</sub>(PO<sub>4</sub>)<sub>2</sub>/BiPO<sub>4</sub> catalyst. *J. Environ. Chem. Eng.* **2019**, *7*, 103075. [[CrossRef](#)]
15. Zhu, J.; Zhou, Y.; Wu, W.; Deng, Y.; Xiang, Y. A Novel Rose-Like CuS/Bi<sub>2</sub>WO<sub>6</sub> Composite for Rhodamine B Degradation. *ChemistrySelect* **2019**, *4*, 11853–11861. [[CrossRef](#)]
16. Wang, D.; Xu, Y.; Sun, F.; Zhang, Q.; Wang, P.; Wang, X. Enhanced photocatalytic activity of TiO<sub>2</sub> under sunlight by MoS<sub>2</sub> nanodots modification. *Appl. Surf. Sci.* **2016**, *377*, 221–227. [[CrossRef](#)]
17. Liu, X.; Xing, Z.; Zhang, Y.; Li, Z.; Wu, X.; Tan, S.; Yu, X.; Zhu, Q.; Zhou, W. Fabrication of 3D flower-like black N-TiO<sub>2</sub>-x@MoS<sub>2</sub> for unprecedented-high visible-light-driven photocatalytic performance. *Appl. Catal. B Environ.* **2017**, *201*, 119–127. [[CrossRef](#)]
18. Saravanan, R.; Karthikeyan, N.; Govindan, S.; Narayanan, V.; Stephen, A. Photocatalytic Degradation of Organic Dyes Using ZnO/CeO<sub>2</sub> Nanocomposite Material under Visible Light. *Adv. Mater. Res.* **2012**, *584*, 381–385. [[CrossRef](#)]
19. Tien, H.N.; Luan, V.H.; Hoa, L.T.; Khoa, N.T.; Hahn, S.H.; Chung, J.S.; Shin, E.W.; Hur, S.H. One-pot synthesis of a reduced graphene oxide–zinc oxide sphere composite and its use as a visible light photocatalyst. *Chem. Eng. J.* **2013**, *229*, 126–133. [[CrossRef](#)]
20. Gao, P.; Ng, K.; Sun, D.D. Sulfonated graphene oxide-ZnO-Ag photocatalyst for fast photodegradation and disinfection under visible light. *J. Hazard. Mater.* **2013**, *262*, 826–835. [[CrossRef](#)]
21. Ramkumar, J.; Chen, Y.; Manigandan, R.; Karpuraranjith, M.; Wang, B.; Li, W.; Zhang, X. A three-dimensional porous CoSnS@CNT nanoarchitecture as a highly efficient bifunctional catalyst for boosted OER performance and photocatalytic degradation. *Nanoscale* **2020**, *12*, 3879–3887.
22. Karpuraranjith, M.; Chen, Y.; Wang, X.; Yu, B.; Rajaboopathi, S.; Yang, D. Hexagonal SnSe nanoplate supported SnO<sub>2</sub>-CNTs nanoarchitecture for enhanced photocatalytic degradation under visible light driven. *Appl. Surf. Sci.* **2020**, *507*, 145026. [[CrossRef](#)]
23. Atchudan, R.; Edison, T.N.J.I.; Perumal, S.; Karthikeyan, D.; Lee, Y.R. Facile synthesis of zinc oxide nanoparticles decorated graphene oxide composite via simple solvothermal route and their photocatalytic activity on methylene blue degradation. *J. Photochem. Photobiol. B Biol.* **2016**, *162*, 500–510. [[CrossRef](#)] [[PubMed](#)]
24. Wu, H.; Tang, Q.; Fan, H.; Liu, Z.; Hu, A.; Zhang, S.; Deng, W.; Chen, X. Dual-Confined and Hierarchical-Porous Graphene/C/SiO<sub>2</sub> Hollow Microspheres through Spray Drying Approach for Lithium-Sulfur Batteries. *Electrochim. Acta* **2017**, *255*, 179–186. [[CrossRef](#)]
25. Wang, B.; Chen, Y.; Wang, X.; Ramkumar, J.; Zhang, X.; Yu, B.; Yang, D.; Karpuraranjith, M.; Zhang, W. rGO wrapped trimetallic sulfide nanowires as an efficient bifunctional catalyst for electrocatalytic oxygen evolution and photocatalytic organic degradation. *J. Mater. Chem. A* **2020**, *8*, 13558–13571. [[CrossRef](#)]
26. Chen, Z.; Zhang, N.; Xu, Y.-J. Synthesis of graphene-ZnO nanorod nanocomposites with improved photoactivity and anti-photocorrosion. *CrystEngComm* **2013**, *15*, 3022–3030. [[CrossRef](#)]
27. Bai, X.; Wang, L.; Zong, R.; Lv, Y.; Sun, Y.; Zhu, Y. Performance Enhancement of ZnO Photocatalyst via Synergic Effect of Surface Oxygen Defect and Graphene Hybridization. *Langmuir* **2013**, *29*, 3097–3105. [[CrossRef](#)]
28. Liu, I.T.; Hon, M.H.; Teoh, L.G. The preparation, characterization and photocatalytic activity of radical-shaped CeO<sub>2</sub>/ZnO microstructures. *Ceram. Int.* **2014**, *40*, 4019–4024. [[CrossRef](#)]
29. Lamba, R.; Umar, A.; Mehta, S.K.; Kansal, S.K. CeO<sub>2</sub>ZnO hexagonal nanodisks: Efficient material for the degradation of direct blue 15 dye and its simulated dye bath effluent under solar light. *J. Alloys Compd.* **2015**, *620*, 67–73. [[CrossRef](#)]
30. Choi, J.; Reddy, D.A.; Islam, M.J.; Ma, R.; Kim, T.K. Self-assembly of CeO<sub>2</sub> nanostructures/reduced graphene oxide composite aerogels for efficient photocatalytic degradation of organic pollutants in water. *J. Alloys Compd.* **2016**, *688*, 527–536. [[CrossRef](#)]

31. Raja, V.R.; Karthika, A.; Kirubahar, S.L.; Suganthi, A.; Rajarajan, M. Sonochemical synthesis of novel ZnFe<sub>2</sub>O<sub>4</sub>/CeO<sub>2</sub> heterojunction with highly enhanced visible light photocatalytic activity. *Solid State Ion.* **2019**, *332*, 55–62. [[CrossRef](#)]
32. Sun, Y.; Lin, H.; Wang, C.; Wu, Q.; Wang, X.; Yang, M. Morphology-controlled synthesis of TiO<sub>2</sub>/MoS<sub>2</sub> nanocomposites with enhanced visible-light photocatalytic activity. *Inorg. Chem. Front.* **2018**, *5*, 145. [[CrossRef](#)]
33. Wang, S.; Zhu, B.C.; Liu, M.J.; Zhang, L.Y.; Yu, J.G.; Zhou, M.H. Direct Z-scheme ZnO/ CdS hierarchical photocatalyst for enhanced photocatalytic H<sub>2</sub>-production activity. *Appl. Catal. B Environ.* **2019**, *243*, 19–26. [[CrossRef](#)]
34. Wolski, P.L.; Grzelak, K.; Munko, M.; Frankowski, M.; Grzyb, T.; Nowaczyk, G. Insight into photocatalytic degradation of ciprofloxacin over CeO<sub>2</sub>/ZnO nanocomposites: Unravelling the synergy between the metal oxides and analysis of reaction pathways. *Appl. Surf. Sci.* **2021**, *563*, 150338. [[CrossRef](#)]
35. Jia, P.; Tan, H.; Liu, K.; Gao, W. Synthesis, characterization and photocatalytic property of novel ZnO/bone char composite. *Mater. Res. Bull.* **2018**, *102*, 45–50. [[CrossRef](#)]
36. Xiao, Y.; Yu, H.; Dong, X. Ordered mesoporous CeO<sub>2</sub>/ZnO composite with photodegradation concomitant photocatalytic hydrogen production performance. *J. Solid State Chem.* **2019**, *278*, 120893. [[CrossRef](#)]
37. Rauf, M.A.; Meetani, M.; Khaleel, A.; Ahmed, A. Photocatalytic degradation of Methylene Blue using a mixed catalyst and product analysis by LC/MS. *Chem. Eng. J.* **2010**, *157*, 373–378. [[CrossRef](#)]
38. Fang, S.; Xin, Y.; Ge, L.; Han, C.; Qiu, P.; Wu, L. Facile synthesis of CeO<sub>2</sub> hollow structures with controllable morphology by template-engaged etching of Cu<sub>2</sub>O and their visible light photocatalytic performance. *Appl. Catal. B Environ.* **2015**, *179*, 458–467. [[CrossRef](#)]
39. Sun, W.; Meng, S.; Zhang, S.; Zheng, X.; Ye, X.; Fu, X.; Chen, S. Insight into the Transfer Mechanisms of Photogenerated Carriers for Heterojunction Photocatalysts with the Analogous Positions of Valence Band and Conduction Band: A Case Study of ZnO/TiO<sub>2</sub>. *J. Phys. Chem. C.* **2018**, *122*, 15409–15420. [[CrossRef](#)]
40. Zhang, X.; Li, R.; Jia, M.; Wang, S.; Huang, Y.; Chen, C. Degradation of ciprofloxacin in aqueous bismuth oxybromide (BiOBr) suspensions under visible light irradiation: A direct hole oxidation pathway. *Chem. Eng. J.* **2015**, *274*, 290–297. [[CrossRef](#)]
41. Zhang, F.; Zhang, Y.; Wang, Y.; Zhu, A.; Zhang, Y. Efficient photocatalytic reduction of aqueous Cr (VI) by Zr<sup>4+</sup> doped and polyaniline coupled SnS<sub>2</sub> nanoflakes. *Sep. Purif. Technol.* **2022**, *283*, 120161. [[CrossRef](#)]
42. Wang, Y.; Su, Y.; Fang, W.; Zhang, Y.; Li, X.; Zhang, G.; Sun, W. SnO<sub>2</sub>/SnS<sub>2</sub> nanocomposite anchored on nitrogen-doped RGO for improved photocatalytic reduction of aqueous Cr(VI). *Powder Technol.* **2020**, *363*, 337–348. [[CrossRef](#)]
43. Gayathri, S.; Jayabal, P.M.; Kottaisamy, M.; Ramakrishnan, V. Synthesis of ZnO decorated graphene nanocomposite for enhanced photocatalytic properties. *J. Appl. Phys.* **2014**, *115*, 173504. [[CrossRef](#)]
44. Ma, D.; Shi, J.W.; Sun, D. Au decorated hollow ZnO@ZnS heterostructure for enhanced photocatalytic hydrogen evolution: The insight into the roles of hollow channel and Au nanoparticles. *Appl. Catal. B Environ.* **2019**, *244*, 748–757. [[CrossRef](#)]
45. Qiao, H.; Huang, Z.; Liu, S.; Tao, Y.; Zhou, H.; Li, M.; Qi, X. Novel Mixed-Dimensional Photocatalysts Based on 3D Graphene Aerogel Embedded with TiO<sub>2</sub>/MoS<sub>2</sub> Hybrid. *J. Phys. Chem. C* **2019**, *123*, 10949–10955. [[CrossRef](#)]
46. Priyadharsan, A.; Vasanthakumar, V.; Karthikeyan, S.; Raj, V.; Shanavas, S.; Anbarasan, P.M. Multi-functional properties of ternary CeO<sub>2</sub>/SnO<sub>2</sub>/rGO nanocomposites: Visible light driven photocatalyst and heavy metal removal. *J. Photochem. Photobiol. A Chem.* **2017**, *346*, 32–45. [[CrossRef](#)]